ELASTIC SCATTERING AND ELECTRON CAPTURE PROCESSES IN COLLISIONS OF $^{3}HE^{2+}$ ION WITH CO MOLECULE BELOW 5 KEV

Abstract

Theoretical investigations have been executed on the process of single electron capture occurring in collisions between 3He2+ ions and CO molecules. Semiclassical collision methods were employed in this study, where adiabatic potentials and nonadiabatic couplings were derived using the multireference single- and double-excitation configuration-interaction (MRDCI) approach. Cross sections for single electron capture, both partial and total, were computed over a range of energies from 0.6 to 6 keV. The calculated results demonstrate a notable sensitivity to molecular configuration, emphasizing a significant steric influence. Notably, the computed single electron capture cross sections closely match the experimental data reported by Kusakabe et al. [Phys. Rev. A 73, 022706 (2006)] and Čadež et al. [J. Phys. B: At. Mol. Opt. Phys. 35, 2515 (2002)]. This study contributes valuable theoretical insights into the underlying collision dynamics, enhancing our comprehension of the experimental measurements.

Keywords: Helium, x-rays, Theoretical investigations, CO molecules

Authors

Ashok Kumar Jha
Department of Physics
Patna Science College
Patna University
Patna, India.
ashok-physics@patnauniversity.ac.in

Shankar Kumar
Department of Physics
Patna Science College
Patna University
Patna, India.

Tinku Kumar
Department of Physics
Patna Science College
Patna University
Patna, India.

I. INTRODUCTION

In recent decades, considerable progress has been achieved in both experimental and theoretical approaches, significantly advancing our understanding of various phenomena occurring within astrophysical plasma [1]. Of particular importance is the phenomenon of electron capture taking place during the interactions between slow, multiply charged ions and atomic or molecular targets. This process plays a crucial role in unraveling the mechanisms accountable for the emission of x-rays and extreme ultraviolet (EUV) photons from astrophysical plasmas [2, 3]. The spectral lines emitted by these multiply charged ions serve as invaluable tools for directly probing the ionization structure of celestial entities.

Cosmic rays and solar wind predominantly consist of protons and doubly ionized helium (He2+), commonly known as α particles. Helium ions have been detected in outer space using an Extreme Ultraviolet (EUV) scanner aboard the Mars Orbiter Planet-B [4]. This EUV satellite has conducted extensive spectroscopic analyses of comets across the Vacuum Ultraviolet (VUV) spectral range [5, 6]. Examination of the observed spectral lines has validated the occurrence of electron capture processes within comets. Among these lines, specific helium spectral lines display remarkable brightness and distinct isolation from others. These particular lines arise from de-excitation following electron capture, leading to excited states of singly charged or neutral helium. The determination of the luminosities of these lines has been achieved through careful observations. However, a profound understanding of the underlying electron capture processes and the subsequent emission of spectral lines is essential for interpreting these observations.

Given that CO molecules constitute a significant portion of the neutral atmosphere of the comet in close proximity to the sun, we have successfully calculated both total and partial cross sections for the collision between He2+ ions and CO molecules, facilitated by the recently recorded He+ emission lines from the comet Hyakutake [5]. These processes align with our areas of interest [7].

$$He2+ + CO \rightarrow He+ (1s\ 2S) + CO+ (\Sigma) + \Delta E \text{ (dissociative)},$$
$$\rightarrow He+ (n \geq 2) + CO+ (\Sigma) \pm \Delta E1 \text{ (non - dissociative)}$$

In this context, "n" represents the principal quantum number, while ΔE and ΔE1 denote the energy deficits pertaining to individual product channels. CO+ (Σ) encompasses the inclusion of final bound or dissociative molecular states. Extensive experimental investigations have been conducted on the collision between He2+ ions and CO molecules [7-12]. However, the corresponding systematic theoretical research has remained somewhat limited [8]. It's worth noting that the alignment between experimental observations and theoretical computations has proven to be unsatisfactory, leading to the absence of a clear explanation for the observed outcomes in previous studies [8].

Thus, in this ongoing inquiry, we have applied the impact-parameter method [13] to scrutinize the single electron capture (SEC) process. The adiabatic potentials and nonadiabatic couplings were ascertained using the multireference single- and double-excitation configuration interaction (MRDCI) approach [14-21]. To ensure the precision of our outcomes, an optimization technique for the atomic basis sets employed in the MRDCI

calculations for multiply charged ions has been implemented. The computation of ion-molecule collisions adheres to the perturbed stationary state (PSS) model [22], where the basis functions are constructed from the molecular orbitals.

The SEC cross sections, both partial and total, have been computed for collision energies ranging from 0.6 to 6 keV, correlating with a solar-wind ion velocity of approximately 3 keV at low heliographic latitudes [23]. A comparison between the calculated electron capture cross sections and existing experimental data [7, 8] reveals that the impact parameter method yields cross sections that closely align with experimental measurements [7, 8] within the energy range considered in this study.

II. THEORETICAL MODELS

1. **Molecular state:** The schematic representation of the collision between the He2+ ion and the CO molecule is depicted in Fig. 1. The He2+ + CO system is characterized using the internal Jacobi coordinates {R, r, α}, with the reference point located at the center of mass of the CO molecule. Employing the MRDCI method [14-21], ab initio calculations have been conducted for three distinct approaches of the He2+ ion toward the CO molecule. In the linear conformation, the He2+ ion approaches the carbon and oxygen ends of the CO molecule at angles of α = 0 and 180°, respectively. For these scenarios, the computations are conducted within the C2v subgroup, which represents the highest Abelian subgroup within the C∞v point group. In the perpendicular approach (α = 90°), the He2+ ion approaches the center of mass of CO in a vertical alignment along the Z-axis. The system exhibits a single symmetry plane in this configuration, namely the YZ plane (belonging to the Cs point group), and the electronic states are categorized based on the two irreducible representations, A' and A", of the Cs point group. In this case, interactions primarily involve radial couplings between A' states, the X component of rotational couplings between A' states, and the Y and Z components of rotational couplings between the A' and A" states. Other interactions are excluded due to symmetry constraints.

   In each of the three approach directions, the reference point for the scattering coordinates is positioned at the center of mass of the [HeCO]2+ system. Within the collision energy range examined in this study, it is noteworthy that the collision time is significantly shorter than the relaxation time of the CO target. Consequently, the molecular state calculations have been executed with the internuclear distance of CO held constant at 2.13222 a0, aligning with the equilibrium configuration of the CO molecule's ground state.

   In this study, a basis set of contracted Cartesian Gaussian functions is used. The basis set of aug-cc-pVQZ [24] for carbon is condensed to [6s, 5p, 4d, 3f, 2g]. It is then enhanced with two diffuse s (αs = 0.0230000 and 0.0055000 a0-2), two diffuse p (αp = 0.021000 and 0.0049000 a0-2), and two diffuse d (αd = 0.0150000 and 0.0032000 a0-2). The basis set for oxygen, aug-cc-pVQZ [24], is contracted to [6s, 5p, 4d, 3f, 2g]. This contracted basis set is then enhanced with two diffuse s (αs = 0.0320000 and 0.0022000 a0-2), two diffuse p (αp = 0.0310000 and 0.0011000 a0-2), and two diffuse d (αd = 0.0150000 and 0.0032000 a0-2). Aug-cc-pVQZ [25] designed for helium uses the basis

set [10s, 5p, 2d, 1f].

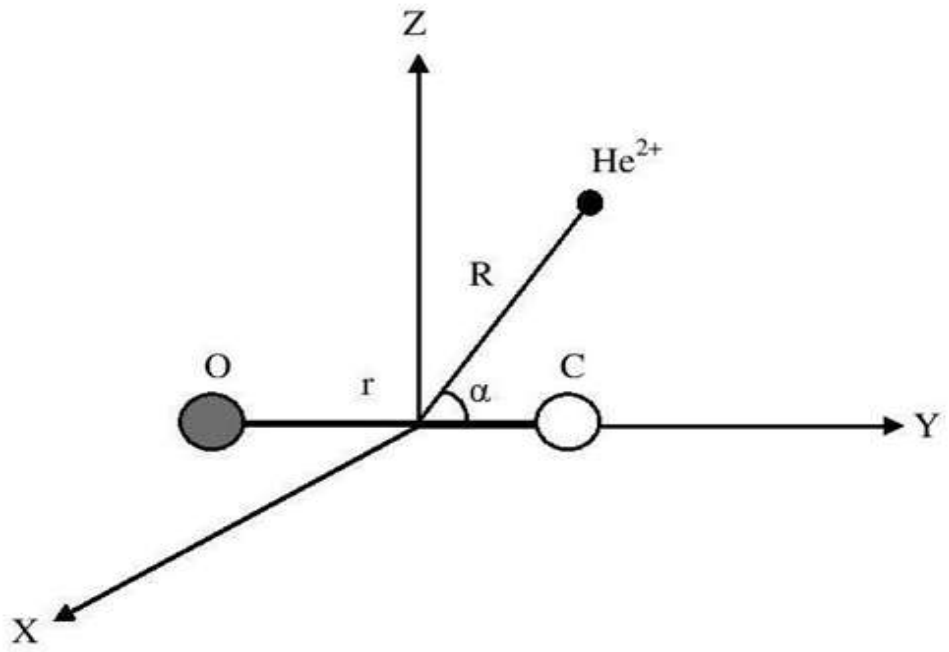

Figure 1: Internal coordinates for the $[HeCO]^{2+}$ system.

For each of the three approach directions, a self-consistent field (SCF) computation was conducted to determine the lowest-energy 1A1 state at various internuclear distances. The resulting molecular orbitals (MOs) from these calculations serve as the orthonormal one-electron basis for the subsequent configuration interaction (CI) analyses.

The adiabatic MRDCI energies have been computed at 173 different internuclear distances within the range of $1.5 \leq R \leq 50.0$ a0, where R represents the distance of He2+ from the center of CO. The MRDCI method was employed, utilizing configuration selection and perturbative energy corrections [14-21].

Table 1: This table provides information on the number of reference configurations (Nref) and the number of roots (Nroot) treated in each irreducible representation, along with the corresponding counts of generated (Ntot) and selected (Nsel) symmetry-adapted functions. These calculations include an analog of the Davidson-Langhoff correction with a threshold of 1.0×10-6 hartree. Please note that R denotes the distance between the He2+ ion and the CO center of mass.

State	Nref	Ntot	Nsel	Nroot	$\Sigma_p c_p^2$
carbon end	R = 2.1 a_0				
$^1A1$	117	25107571	152860	8	0.91925
$^1B1$	131	36530868	130437	5	0.91400
$^1A2$	58	19913451	100128	4	0.91925
$^3A1$	122	56874767	132811	6	0.91783
$^3B1$	131	66373749	123435	5	0.91880
$^3A2$	58	36315855	100829	4	0.91825
oxygen end	R = 2.7 a_0				
$^1A1$	108	24130542	159236	8	0.92560
$^1B1$	72	19081874	141719	5	0.92100
$^1A2$	41	12479242	114371	4	0.91875
$^3A1$	113	54168588	128649	6	0.92980
$^3B1$	124	65232445	150152	5	0.92960
$^3A2$	70	46421304	119775	4	0.92790
center of mass	R = 3.5 a_0				
$^1A'$	214	76191198	193952	10	0.92620
$^1A''$	127	60828104	160514	6	0.92050
$^3A'$	217	149263062	201955	10	0.92740
$^3A''$	154	134429332	149371	6	0.92616

After an initial analysis of the wave functions associated with the lowest roots of a specific symmetry at various representative internuclear distances, a group of reference configurations is chosen. To effectively categorize the generated configurations, a selection threshold of T = 1.0 × 10-6 hartree is applied, discerning them based on their ability to reduce the total energy of a specific root compared to what is achieved in the reference secular equations with smaller configurations. Detailed information regarding the counts of reference configurations, selected roots, and the respective sizes of the generated and selected CI spaces can be found in Table I. These calculations are conducted within the C2v subgroup of the C∞v point group, although the molecular orbitals themselves adhere to the irreducible representations of D∞h linear symmetry, facilitating the identification of resulting CI eigenfunctions.

The configuration interaction (CI) treatment was conducted using the Table CI method [19-21] to efficiently address various open-shell situations that arise due to single and double substitutions in relation to the reference configurations. Table I also provides the sums of squared coefficients of reference configurations Σp cp2 for each of the lowest roots, which serves as an indicator of the appropriateness of the chosen reference species in each case. Typically, values in the range of 0.929–0.914 were observed, falling within an acceptable range for CI treatments involving only ten active electrons (since the carbon 1s shell and oxygen 1s shell are always doubly occupied). These Σp cp2 values were also utilized in the multireference analogue to the Davidson correction [26, 27] for estimating the impact of higher excitations on the energy of each root, consequently obtaining a reasonably accurate full CI energy.

The computed first ionization potential of the CO molecule, resulting in CO+ (2Σ+), is determined to be 13.6692 eV, demonstrating good agreement with the experimental value of 13.99 eV obtained through photoelectron spectroscopy [28]. Energy differences between the single electron capture channel, He+ (1s 2S) + CO+ (X 2Σ+), and the entry channel, He2+ + CO (X 1Σ+), at R = 50 a0 are calculated to be 2.20786 and 2.24599 eV when the He2+ ion approaches the carbon and oxygen ends, respectively. Regarding the triplet manifold, the calculated energy differences for the single electron capture channel, He+ (1s 2S) + CO+ (X 2Σ+), and the entry channel, He2+ + CO (X 3Σ+), are 9.2834 and 9.2913 eV for the He2+ ion approaching the carbon and oxygen ends, respectively. However, for the perpendicular approach, the asymptotic energy difference could not be computed since the entry channel lies significantly above the calculated adiabatic potentials.

Utilizing the optimized basis, the radial coupling matrix elements between all pairs of states of the same symmetry have been computed through the application of a finite-difference method [29].

$$A_{ij} = \langle \psi_i | \frac{\partial}{\partial R} | \psi_j \rangle = \lim_{\Delta R \to 0} \frac{1}{\Delta R} \langle \psi_i(R) \mid \psi_i(R + \Delta R) \rangle,$$

With a step size of 0.0002 a_0 and the electronic coordinate origin at the center of mass of the $[HeCO]^{2+}$ system. The rotational couplings between states of angular momentum $\Delta\Lambda = \pm 1$ have been calculated from the angular momentum tensor using a standard procedure [30].

2. **Scattering calculation:** The scattering calculation was conducted within the keV energy range, where it has been established that straight-line trajectories yield satisfactory results [31]. The computations were carried out using the EIKONX program [13], which relies on an efficient propagator method [33], and semiclassical approaches were applied with a high degree of accuracy [32].

For He2+ ions with keV-level energy, the collision times are approximately on the order of 10^(-16) seconds. In contrast, the timescales for molecular rotation and vibration are typically around 10^(-11) and 10^(-14) seconds, respectively [34]. Consequently, it is reasonable to assume that the internuclear distance between the C and O atoms remains constant during the collision event, allowing for the application of the Franck–Condon (FC) principle. This assumption is valid since the times for molecular rotation and vibration are significantly longer than the collision time. Therefore, cross sections related to purely electronic transitions can be determined by solving the impact parameter equation, following the standard ion-atom approach, while considering the fixed internuclear distance of the molecular target in a given geometry.

The electronic transitions occurring between the molecular states are predominantly influenced by nonadiabatic radial and rotational coupling matrix elements. Consequently, the coupled equations have been systematically solved, considering all relevant radial and rotational couplings. In this specific investigation, electron translation factors (ETFs) have been integrated, a common practice to ensure that the cross sections remain independent of the choice of coordinate origin. These ETFs have been evaluated using an approximation involving common translation factors (CTFs) [35]. While the impact of ETFs is expected to be minimal within the energy range examined in this study, their inclusion ensures the fulfillment of correct scattering boundary conditions.

The influence of spin-orbit couplings is expected to be low in the range of energy considered in the present work. Hence, singlet and triplet states have been considered separately. Singlet states included in the dynamical calculations are: the entry channel 2 $^1\Sigma^+$ [He^{2+} + CO ($X\ ^1\Sigma^+$)] and SEC channels: 1 $^1\Sigma^+$ [He^+ (1*s* ^2S) + CO^+ ($X\ ^2\Sigma^+$)], 3 $^1\Sigma^+$ [He^+ (*n*=2) + CO^+ ($X\ ^2\Sigma^+$)], 4 $^1\Sigma^+$ [He^+ (*n*=3) + CO^+ ($X\ ^2\Sigma^+$)], 5 $^1\Sigma^+$ [He^+ (*n*=3) + CO^+ ($A\ ^2\Sigma^+$)], 1 $^1\Pi$ [He^+ (*n*=2) + CO^+ ($A\ ^2\Pi$), 2 $^1\Pi$ [He^+ (*n*=3) + CO^+ ($A\ ^2\Pi$)]. Triplet states included in the dynamical calculations are: the entry channel 5 $^3\Sigma^+$ [He^{2+} + CO ($X\ ^3\Sigma^+$)] and SEC channels: 1 $^3\Sigma^+$ [He^+ (1*s* ^2S) + CO^+ ($X\ ^2\Sigma^+$)], 2 $^3\Sigma^+$ [He^+ (1*s* ^2S) + CO^+ ($A\ ^2\Sigma^+$)], 3 $^3\Sigma^+$ [He^+ (*n*=2) + CO^+ ($X\ ^2\Sigma^+$)], 4 $^3\Sigma^+$ [He^+ (*n*=2) + CO^+ ($A\ ^2\Sigma^+$)], 1 $^3\Pi$ [He^+ (1*s* ^2S) + CO^+ ($A\ ^2\Pi$)], 2 $^3\Pi$ [He^+ (*n*=2) + CO^+ ($A\ ^2\Pi$)].

III. RESULTS

1. **Adiabatic potentials and nonadiabatic couplings:** Rotational couplings have been taken into account with respect to the symmetries of the entry channels (1Σ+ and 3Σ+),

which means that 1Π and 3Π states have also been incorporated into the collision dynamics. The adiabatic potential energy curves illustrate the scenarios when the He2+ ion approaches the oxygen end of the CO molecule at an angle of 180° (singlet states) and are depicted in Fig. 2. Specifically, the 2 1Σ+ state represents the He2+/CO entry channel, while all the other states are associated with the He+/CO+ single electron capture channels.

The 1 1Σ+ and 2 1Σ+ states exhibit an avoided crossing within the range of R = 8 to 9 a0 when the He2+ ion approaches the oxygen end of the CO molecule. Conversely, for the carbon end (α = 0°), these avoided crossings are observed beyond R = 9.5 a0. In the case of the 2 1Σ+ and 3 1Σ+ states, an avoided crossing near R = 2.2 a0 is evident for the carbon end, while minimal or no avoided crossing occurs between these states for the oxygen end of the CO molecule. Both termini display multiple avoided crossings for the 4 1Σ+ and 5 1Σ+ states, indicating their significant role in the SEC process during high-energy collisions. Curve crossings between the entry channel 2 1Σ+ and SEC channel 1 1Π suggest a substantial contribution from the 1 1Π state in the SEC process, while curve crossings between the 2 1Π state and the high-lying 4 1Σ+ and 5 1Σ+ states contribute to flux redistribution in high-energy collisions. In the case of triplet states, the adiabatic potentials for He2+ ions approaching the oxygen end of the CO molecule are shown in Fig. 3. The entry channel (He2+/CO) is represented by the 5 3Σ+ state, while all other states correspond to SEC (He+/CO+) channels. Similar to the singlet states, the adiabatic potentials for triplet states exhibit distinct characteristics for both termini (carbon and oxygen). For the oxygen end, the 5 3Σ+ and 4 3Σ+ states display a strong avoided crossing near R = 2.8 a0, along with several smoothly avoided crossings within the ranges of R = 3.5 - 4 a0, 4.5 - 5.5 a0, and beyond 9 a0. Conversely, for the carbon end (α = 0°), these states demonstrate a smooth avoided crossing below R = 2 a0, a very weak avoided crossing near R = 5.5 a0, and a weak avoided crossing around R = 10 a0. Furthermore, the 3 3Σ+ and 4 3Σ+ states for the carbon-end approach exhibit strong avoided crossings near R = 2.2, 4.1, and 7.5 a0, while for the oxygen end, these states (5 3Σ+ and 4 3Σ+) undergo a smooth avoided crossing below R = 2.5 a0, and a strong avoided crossing near R = 4.2, 6.0, and 6.5 a0. In both cases, the 3 3Σ+, 2 3Σ+, and 1 3Σ+ states exhibit minimal or no avoided crossings.

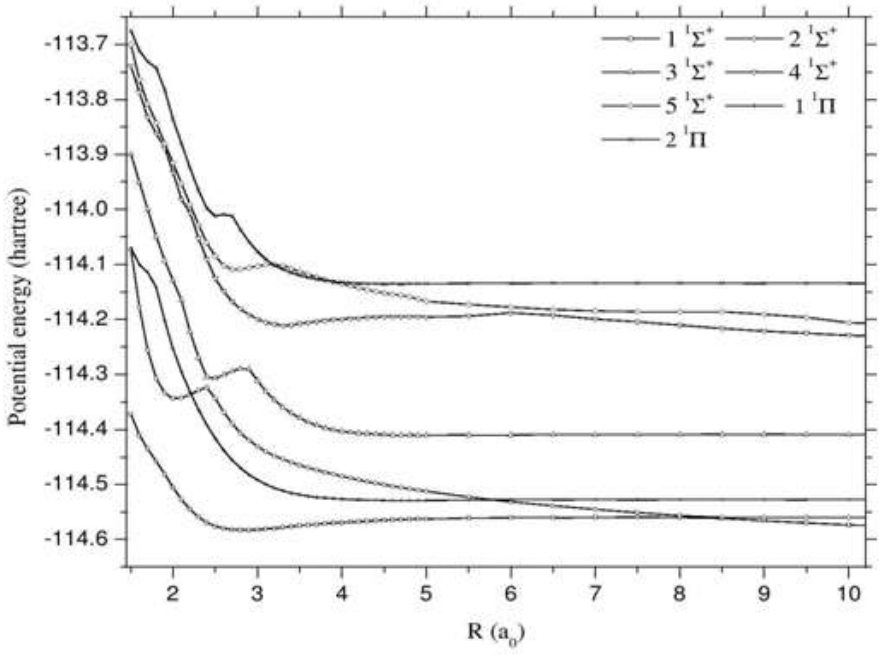

Figure 2: Adiabatic potential energy curves for the $^{1}\Sigma^{+}$ and $^{1}\Pi$ (singlet) states of the $[HeCO]^{2+}$ system at equilibrium, $\alpha = 180°$.

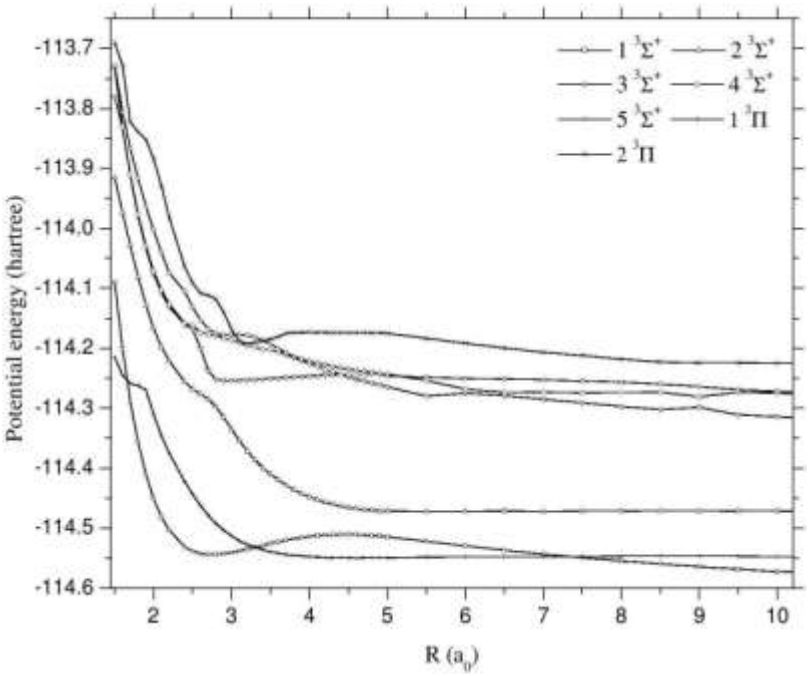

Figure 3: Adiabatic potential energy curves for the $^{3}\Sigma^{+}$ and $^{3}\Pi$ (triplet) states of the $[HeCO]^{2+}$ system at equilibrium, $\alpha = 180°$.

The intersections between the 2 3Π and 5 3Σ+ states indicate the substantial involvement of the 2 3Π state in the SEC process, while the crossings between the 1 3Π

and 1 3Σ+ states contribute significantly to flux redistribution. In both singlet and triplet states, the degree of mixing is relatively less pronounced when the He2+ ion approaches the carbon end compared to the oxygen end of the CO molecule. Consequently, a prominent steric effect is anticipated to have a significant impact on the SEC process.

In the adiabatic potential energy curves for the He2+ ion when approaching the center of mass (α = 90°) of the CO molecule, the ground state entry channel (He2+/CO) is positioned significantly higher than the calculated potentials. Consequently, it has been excluded from the scattering calculation.

Considering the multitude of channels involved in the current calculation and the notable differences in radial couplings between adjacent and non-adjacent states, only the radial couplings for adjacent channels of the 1Σ+ (singlet) and 3Σ+ (triplet) states are presented here for illustrative purposes. The radial couplings for the adjacent 1Σ+ (singlet) and 3Σ+ (triplet) states as the He2+ ion approaches the oxygen end (α = 180°) of the CO molecule are depicted in Figs. 4 and 5, respectively. These figures reveal significant variations in the positions, characteristics, and magnitudes of the radial couplings as the orientation of the He2+ projectile with respect to the CO molecule changes.

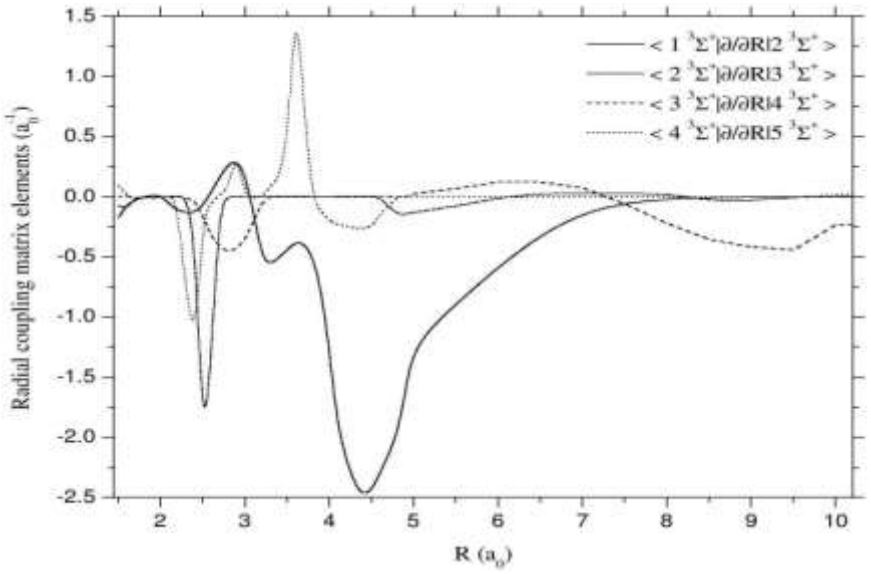

Figure 4: Nonadiabatic radial couplings for the adjacent $^{1}\Sigma^{+}$ (singlet) states of the $[HeCO]^{2+}$ system at equilibrium, α = 180°.

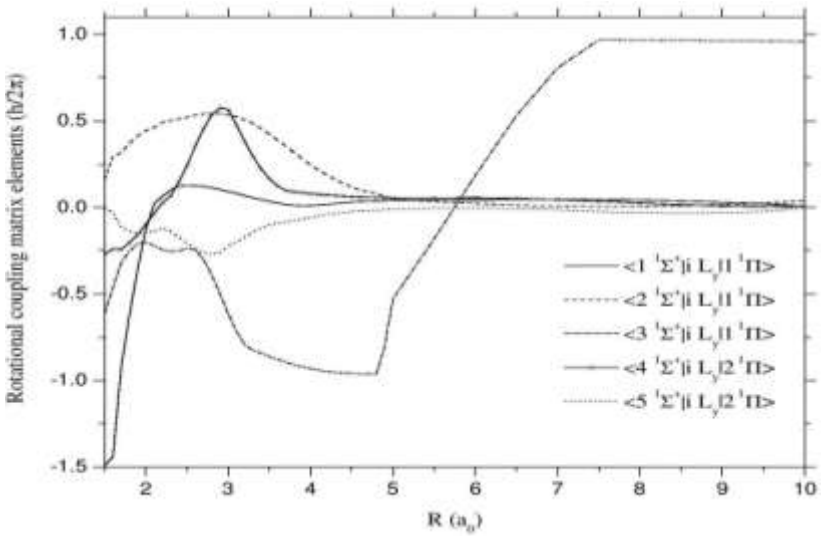

Figure 5: Nonadiabatic radial couplings for the adjacent $^{3}\Sigma^{+}$ (triplet) states of the $[HeCO]^{2+}$ system at equilibrium, $\alpha = 180°$.

The rotational couplings between the adjacent 1,3Σ+ and 1,3Π states at the oxygen end ($\alpha = 180°$) of the CO molecule are depicted in Figs. 6 and 7 for the singlet and triplet states, respectively. Notably, rotational couplings between two states corresponding to molecular fragments with the same number of electrons, such as < 3 1Σ+| iLy | 1 1Π> and < 2 3Σ+| iLy | 1 3Π>, maintain a constant finite value as R becomes large. Conversely, for states corresponding to molecular fragments with different configurations, like < 1 1Σ+| iLy | 1 1Π> and < 1 3Σ+| iLy | 1 3Π>, the rotational couplings tend to zero as R increases. It's worth noting that due to nonadiabatic interactions between adjacent states, the rotational couplings exhibit non-smooth behavior near the avoided crossings.

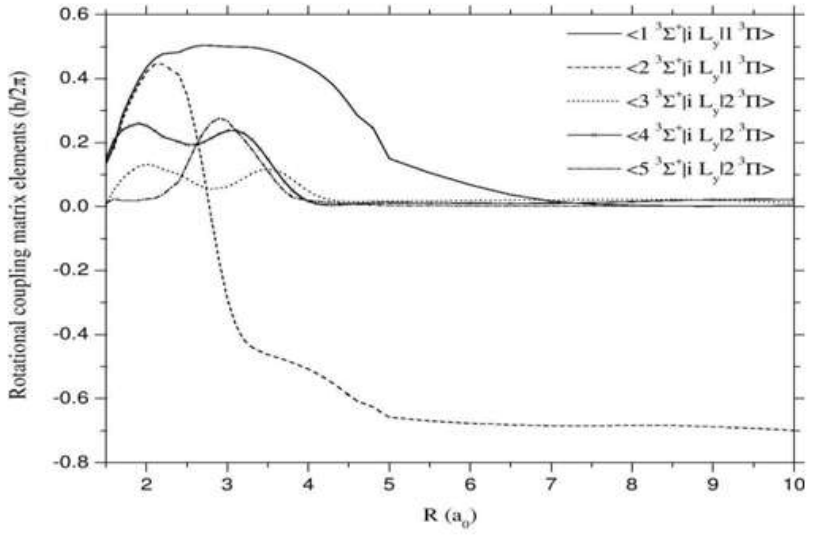

Figure 6: Nonadiabatic rotational couplings for the adjacent $^{1}\Sigma^{+}$ and $^{1}\Pi$ (singlet) states of the $[HeCO]^{2+}$ system at equilibrium, $\alpha = 180°$.

IV. CROSS SECTIONS

The collision dynamics of the [HeCO]2+ system were carried out within an energy range spanning from 0.6 to 6.0 keV. Within this energy range, spin-orbit effects were omitted, leading to separate consideration of the triplet and singlet manifolds. It's worth noting that based on statistical weight, the triplet manifold constitutes 3/4 of the population of the ground state entry channel, whereas the singlet manifold represents 1/4 of the population. In order to assess the impact of molecular orientation on cross sections, the calculations were conducted for He2+ ions approaching both the carbon and oxygen termini of the CO molecule.

1. **Partial cross sections for each individual level:** The partial single electron capture (SEC) cross sections involving He2+ ions approaching the oxygen end (α = 180°) of the CO molecule, particularly in singlet states, are depicted in Figure 8. Regardless of the orientation of the He2+ projectile in relation to the CO molecule, the 1 1Σ+ state [He+ (1s 2S) + CO+ (X 2Σ+)] exhibits a predominant contribution to the SEC process at energies below 3 keV. This underscores the vital role played by radial coupling matrix elements between the 1 1Σ+ state and the entry channel 2 1Σ+ [He2+ + CO (X 1Σ+)] during low-energy collisions. The 3 1Σ+ state [He+ (n=2) + CO+ (X 2Σ+)] also becomes increasingly significant in the SEC process as collision energy rises, reflecting the heightened contribution of radial coupling matrix elements between the 3 1Σ+ state and the entry channel 2 1Σ+ with increasing collision energy.

   At the carbon end (α = 0°), the 1 1Π state [He+ (n=2) + CO+ (A 2Π)] similarly plays a notable role in the SEC process, and its contribution increases as collision energy escalates. This phenomenon is mirrored in the rotational coupling matrix element between the 1 1Π state [He+ (n=2) + CO+ (A 2Π)] and the 2 1Σ+ entry channel. Conversely, the contribution of the 1 1Π state is relatively subdued in the SEC process for the oxygen end (α = 0°), but it becomes more prominent in high-energy collisions.

   In both orientations, the SEC channels 4 1Σ+ [He+ (n=3) + CO+ (X 2Σ+)], 5 1Σ+ [He+ (n=3) + CO+ (A 2Σ+)], and 5 1Π [He+ (n=3) + CO+ (A 2Π)] exhibit a secondary role in the SEC process during low- to intermediate-energy collisions. However, for the oxygen end, the 5 1Π state assumes a significant role in the SEC process during intermediate- to high-energy collisions.

   Partial SEC cross sections for He^{2+} ion approaching the oxygen end (triplet states) are shown in Fig. 9. The 1 $^{3}\Pi$ [He^{+} (1*s* ^{2}S) + CO^{+} (*A* $^{2}\Pi$)] state has a dominant contribution in the

   SEC process and it increases with collision energy. Hence, rotational coupling matrix elements between the 1 $^{3}\Pi$ state and the entry channel 6 $^{3}\Sigma^{+}$ [He^{2+} + CO (*X* $^{3}\Sigma^{+}$)] are seen to play an important role. The 4 $^{3}\Sigma^{+}$ [He^{+} (*n*=2) + CO^{+} (*X* $^{2}\Sigma^{+}$)] state has an important contribution in the SEC process and shows a low dependence on collision energy below 4 keV. Thus, radial coupling matrix elements between the 4 $^{3}\Sigma^{+}$ state and the entry channel 6 $^{3}\Sigma^{+}$ have a significant contribution in the SEC process in high-energy collisions. The SEC channels, 1 $^{3}\Sigma^{+}$ [He^{+} (1*s* ^{2}S) + CO^{+} (*X* $^{3}\Sigma^{+}$)] and 2 $^{3}\Sigma^{+}$ [He^{+} (1*s* ^{2}S) +

CO^+ ($A\ ^2\Sigma^+$)], have a significant contribution in the electron capture process but their contribution decreases with collision energy. The 5 $^3\Sigma^+$ [He^+ (n=2) + CO^+ ($A\ ^2\Sigma^+$)] state has only a small contribution in low-energy collisions but it increases with collision energy. The 5 $^3\Pi$ [He^+ (n=2) + CO^+ ($A\ ^2\Pi$)] state plays a secondary role in the SEC process in low- to intermediate-energy collisions.

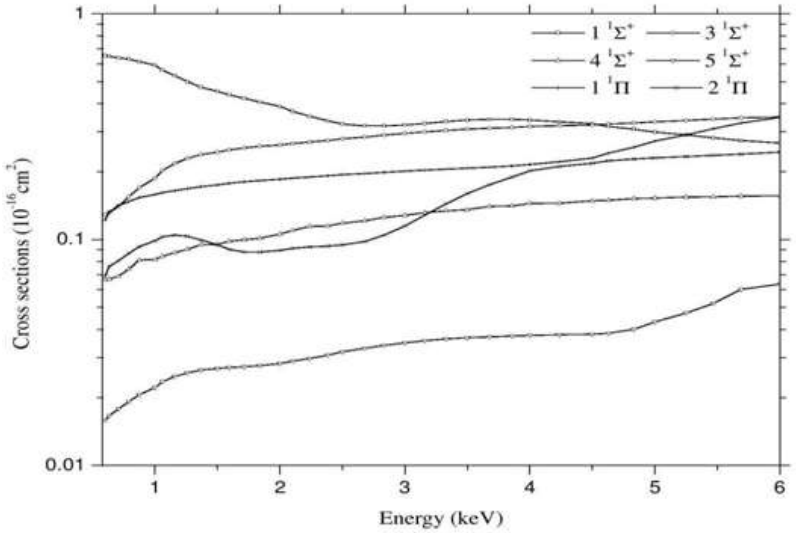

Figure 8: Partial SEC cross sections for the $^1\Sigma^+$ and $^1\Pi$ (singlet) states of the $[HeCO]^{2+}$ system at equilibrium, α = 180°.

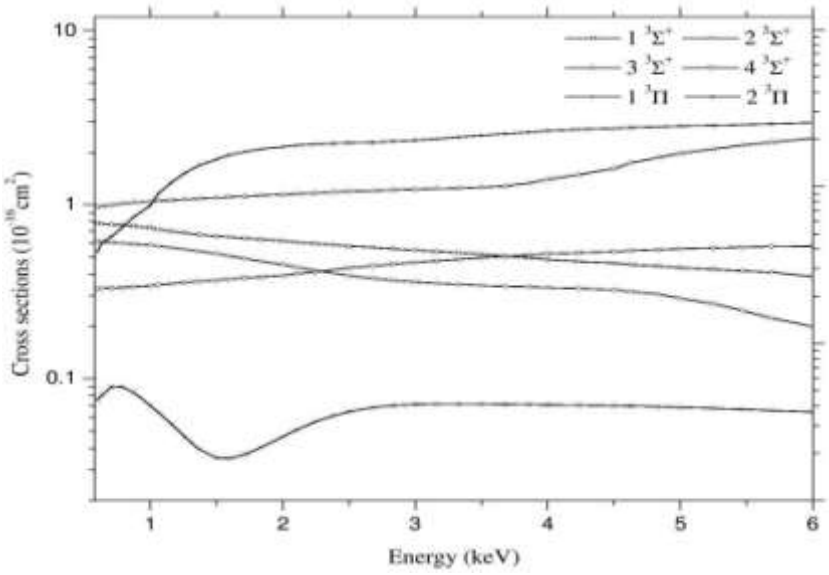

Figure 9: Partial SEC cross sections for the $^3\Sigma^+$ and $^3\Pi$ (triplet) states of the $[HeCO]^{2+}$ system at equilibrium, α = 180°.

In the context of partial single electron capture (SEC) cross sections for He2+ ions approaching the carbon end, particularly in triplet states, the 1 3Π state [He+ (1s 2S)

+ CO+ (A 2Π)] emerges as the dominant contributor to the SEC process. This contribution intensifies as collision energy increases, underscoring the pivotal role played by rotational coupling matrix elements between the 1 3Π state and the entry channel 5 3Σ+ [He2+ + CO (X 3Σ+)] in driving the SEC process. The 4 3Σ+ state [He+ (n=2) + CO+ (X 2Σ+)] exerts a minor influence on the SEC process, exhibiting a weak dependence on collision energy below 3.5 keV. Beyond this threshold, the contribution of the 4 3Σ+ state gains significance with escalating collision energy, highlighting the substantial contribution of the radial coupling matrix element between the 4 3Σ+ state and the entry channel 5 3Σ+ to the SEC process in high-energy collisions.

The 2 3Σ+ state [He+ (1s 2S) + CO+ (A 2Σ+)] exerts a limited impact on the SEC process, with its contribution increasing as collision energy rises below 2 keV. However, above this energy threshold, the influence of the 2 3Σ+ state in the SEC process demonstrates very marginal dependence on collision energy. In contrast, the 1 3Σ+ state [He+ (1s 2S) + CO+ (X 3Σ+)], 5 3Σ+ [He+ (n=2) + CO+ (A 2Σ+)], and 5 3Π [He+ (n=2) + CO+ (A 2Π)] states contribute minimally to the SEC process during low- to intermediate-energy collisions.

The oscillations observed in partial cross sections of these states arise due to interferences between these states. The computed partial cross sections reveal that the He+ (1s 2S) state plays a crucial role in the single electron capture (SEC) process during low- to intermediate-energy collisions, while the He+ (n=2) state significantly contributes to intermediate- to high-energy collisions. These findings align well with the experimental results reported by Kearns et al. [7]. Although it was not feasible to calculate partial cross sections for the perpendicular approach ($\alpha = 90°$) of He2+ ions toward the CO molecule, the partial cross sections obtained for the two distinct modes of approach, namely, the carbon and oxygen termini, underscore the presence of a pronounced steric effect in the collision dynamics.

2. **Total Cross Sections:** In Figure 10, you can observe the total single electron capture (SEC) cross sections for He2+ ions approaching both the carbon and oxygen termini of the CO molecule. The total electron capture cross sections exhibit an upward trend with increasing collision energy for the oxygen end, whereas for the carbon end, the total electron capture cross sections show a gradual increase with collision energy. These curves clearly illustrate that the SEC process is more favorable toward the oxygen end. Consequently, it becomes evident that the calculated SEC cross sections are significantly influenced by the molecular orientation.

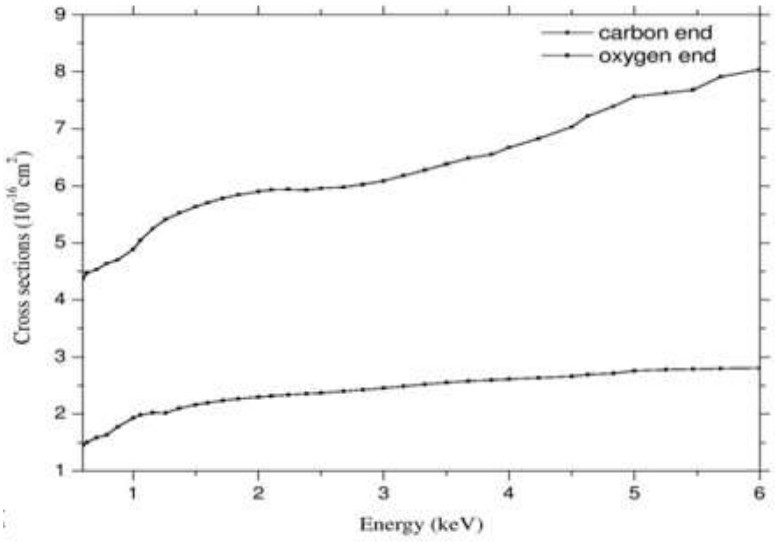

Figure 10: Total SEC cross sections for different orientations of the He^{2+} projectile towards CO molecule at equilibrium

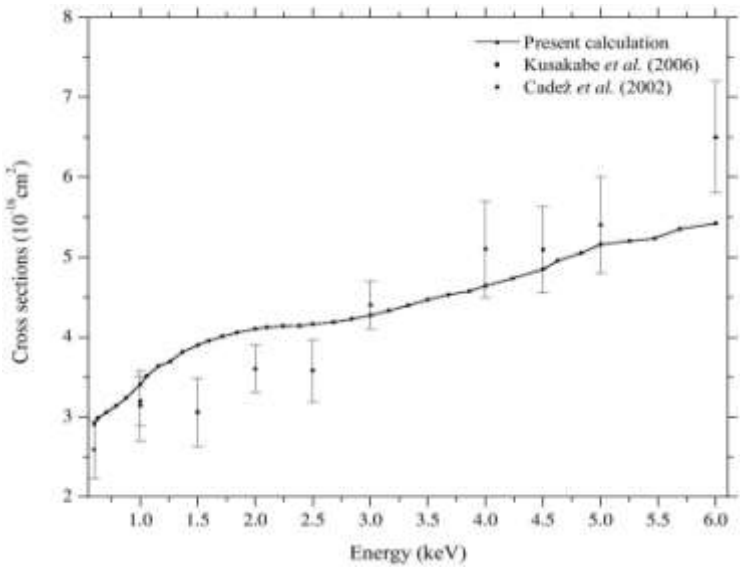

Figure 11: Total SEC cross sections averaged over two different orientations of the He^{2+} projectile towards CO molecule at equilibrium; filled circles with solid line, the present calculation; filled rectangles with error bars, the measurements of Kusakabe *et al.* [8]; filled triangles with error bars, the measurements of Čadež *et al*. [9].

Finally, let's juxtapose the computed total single electron capture (SEC) cross sections, averaged over two molecular orientations (carbon and oxygen termini), with the experimental measurements conducted by Kusakabe et al. [8] and Čadež et al. [9], as illustrated in Figure 11. Overall, there is very good agreement between the results of our calculations and the two sets of experimental data. Across the energy range examined in this study, our calculated SEC cross sections display an increase with collision energy, a

trend that aligns both qualitatively and quantitatively with the experimental findings. Notably, the previously reported theoretical results by Kusakabe et al. [8] were approximately 50% lower than their experimental measurements. Therefore, the SEC cross sections derived in this study represent a substantial improvement over prior theoretical calculations. It is anticipated that the agreement between theoretical and experimental outcomes will further improve when SEC cross sections for the perpendicular approach of the He2+ ion toward the CO molecule are incorporated.

3. **Fragmentation:** While the present study did not conduct a rigorous analysis of the fragmentation of the CO molecule resulting from the impact of He2+ ions, we provide a brief overview of potential mechanisms and consequences associated with fragmentation processes. In collisions between He2+ ions and CO molecules, the energy difference between the entry channel He2+ + CO (X 1Σ+) and the single electron capture (SEC) channel He+ (1s 2S) + CO+ [dissociative states] spans from 0 to 20 eV [7]. The energy difference between the entry channel (He2+/CO) and the SEC channel, He+ (n=2) + CO+ (X 2Σ+), is relatively small (approximately -0.42 eV) [7]. Radial coupling matrix elements between the entry channel and single electron capture [He+ (1s 2S) + CO+] channels are significant. Consequently, electron capture into the [He+ (1s 2S) + CO+] channel is highly efficient in low-energy collisions.

   The specific outcome of the electron capture process depends on the energy transferred to CO+ during the collision. The lowest-energy state of CO+ possesses a binding energy of approximately 8.3 eV [36] and an equilibrium internuclear distance nearly identical to that of the CO ground state. In accordance with the Franck–Condon (FC) principle, it is probable that most of the CO+ ions generated through SEC into the He+ (n=2) state will populate the low-lying bound states of CO+ that are relatively stable. In contrast, SEC into the He+ (1s 2S) state results in the formation of an unstable CO+ ion, leading to its dissociation. The dissociation of the CO+ ion formed through single electron capture into the He+ (1s 2S) state gives rise to the generation of either C+ or O+ ions.

   As reported by Shah and Gilbody [37], in collisions between He2+ ions and CO molecules at 32 keV, the lowest energy considered in their study, dissociative SEC channels contribute to a total cross section of $5.05\times10-16$ cm2, compared to a total of $11.9\times10-16$ cm2 from non-dissociative SEC. They also observed that dissociative electron capture leads to the formation of He+ + C+ + O+ + e-, He+ + C2+ + O + e-, He+ + C2+ + O+ + 2e-, and He+ + C2+ + O2+ + 3e-. At 12 keV, Folkerts et al. [38] found that fragmentation channels account for approximately 46% of the total products resulting from the ionization of CO.

V. CONCLUSIONS

The collision dynamics of the [HeCO]2+ system have been scrutinized utilizing the impact parameter method [13] across an energy spectrum ranging from 0.6 to 6.0 keV, corresponding to ion velocities typically around 3 keV in the context of solar-wind ions at low heliographic latitudes [23]. Partial and total single electron capture (SEC) cross sections have been computed, considering the statistical weights of 1/4 and 3/4 for the singlet and

triplet manifolds, respectively. To investigate the impact of molecular orientation on these computed cross sections, the calculations have been performed for scenarios where the He2+ ion approaches both the carbon and oxygen ends of the CO molecule. The predominance of the oxygen end in facilitating the electron capture process has been underscored. Additionally, we have presented the partial and total SEC cross sections, which have been averaged over the two molecular orientations (carbon and oxygen termini) considered in this study.

The orientation-averaged total cross sections for both single and double electron capture, as computed in this investigation, have been juxtaposed with the available experimental data. It has been demonstrated that the impact parameter method produces cross section values that closely align with the experimental observations [8, 9], particularly within the energy range explored in this research. The primary importance of dissociative single electron capture in low-energy collisions has been emphasized. Moreover, the discourse has centered on the process of single electron capture into He+ (1s 2S) states, leading to the formation of unstable CO+ ions and their subsequent fragmentation, resulting in the generation of multiply charged ions. The calculated partial and total SEC cross sections underscore the substantial influence of radial and rotational couplings relative to spin-orbit couplings. These factors have been shown to impact processes occurring in the cometary atmosphere that give rise to X-ray and EUV photon emissions. The SEC cross section data presented in this study are anticipated to be valuable for various applications.

REFERENCES

[1] S. Lepp, P. C. Stancil, and A. Dalgarno, J. Phys. B: At. Mol. Opt. Phys. 35, R57 (2002).
[2] T. R. Kallman and P. Palmeri, Rev. Mod. Phys. 79, 79 (2007).
[3] A. Bhardwaj, R. F. Elsner, G. R. Gladstone, T. E. Cravens, C. M. Lisse, K. Dennerl, G. Branduardi-Raymont, B. J. Wargelin, J. H. Waite Jr., I. Robertson, N. Østgaard, P. Beiersdorfer, S. L. Snowden, and V. Kharchenko, Planet. Space Sci. 55, 1135 (2007).
[4] I. Yoshikawa, A. Yamazaki, K. Shiomi, M. Nakamura, K. Yamashita, Y. Saito, M. Hirahara, Y. Takizawa, W. Miyake, and S. Matsuura, J. Geophys. Res. 106, 26057 (2001).
[5] V. A. Krasnoplosky and M. J. Mumma, Astrophys. J. 549, 629 (2001).
[6] V. A. Krasnopolsky, M. J. Mumma, M. Abbott, B. C. Flynn, K. J. Meech, D. K. Yeomans, P. D. Feldman, and C. B. Cosmovici, Science 277, 1488 (1997).
[7] D. M. Kearns, D. R. Gillen, D. Voulot, J. B. Greenwood, R. W. McCullough, and H. B. Gilbody, J. Phys. B: At. Mol. Opt. Phys. 34, 3401 (2001).
[8] T. Kusakabe, Y. Miyamoto, M. Kimura, and H. Tawara, Phys. Rev. A 73, 022706 (2006).
[9] I. Čadež, J. B. Greenwood, A. Chutjian, R. J. Mawhorter, S. J. Smith, and M. Niimura, J. Phys. B: At. Mol. Opt. Phys. 35, 2515 (2002).
[10] K. Ishii, K. Okuno, and N. Kobayashi, Phys. Scr. T 80, 176 (1999).
[11] M. E. Rudd, T. V. Goffe, and A. Itoh, Phys. Rev. A 32, 2128 (1985).
[12] M. Albu, L. Mrazek, F. Aumayr, and H. Winter, Int. J. Mol. Sci. 3, 209 (2002).
[13] R. J. Allan, C. Courbin, P. Salas, and P. Wahnon, J. Phys. B: At. Mol. Opt. Phy. 23, L461 (1990).
[14] R. J. Buenker, and S. D. Peyerimhoff, Theor. Chim. Acta (Berl.) 35, 33 (1974).
[15] R. J. Buenker, and S. D. Peyerimhoff, Theor. Chim. Acta (Berl.) 39, 217 (1975).
[16] R. J. Buenker, Int. J. Quantum Chem. 29, 435 (1986).
[17] R. J. Buenker, in *Proceedings of the Workshop on Quantum Chemistry and Molecular Physics*, edited by P. G. Burton (University of Wollongong Press, Wollongong, Australia, 1980), p. 1.5.1.
[18] R. J. Buenker, in *Current Aspects of Quantum Chemistry 1981*, edited by R. Carbo, Studies in Physical and Theoretical Chemistry Vol. 21 (Elsevier, Amsterdam, 1982), p.17 and 81.
[19] R. J. Buenker and R. A. Phillips, J. Mol. Struct. (THEOCHEM) 123, 291 (1985).
[20] S. Krebs and R. J. Buenker, J. Chem. Phys. 103, 5613 (1995).

[21] R. J. Buenker and S. Krebs, in *Recent Advances in Multireference Methods*, edited by K. Hirao (World Scientific, Singapore, 1999), p. 1.J. B. Delos, Rev. Mod. Phys. 53, 287 (1981).
[23] N. A. Schwadron, and T. E. Cravens, Astrophys. J. 544, 558 (2000).
[24] R. A. Kendall, T. H. Dunning and R. J. Harrison, J. Chem. Phys. 96, 6796 (1992).
[25] D. E. Woon and T. H. Dunning, J. Chem. Phys. 100, 2975 (1994).
[26] S. R. Langhoff and E. R. Davidson, Int. J. Quantum Chem. 7, 759 (1973).
[27] P. J. Bruna, S. D. Peyerimhoff, and R. J. Buenker, Chem. Phys. Lett. 72, 278 (1980).
[28] K. Kimura, S. Katsumata, Y. Achiba, T. Yamazaki, and S. Iwata, *Handbook of He I Photoelectron Spectra of Fundamental Organic Molecules* (Japan Scientific Society, Tokyo, 1981).
[29] G. Hirsch, P. J. Bruna, R. J. Buenker, and S. D. Peyerimhoff, Chem. Phys. 45, 335 (1980).
[30] M. Kimura, Y. Li, G. Hirsch, and R. J. Buenker, Phys. Rev. A 52, 1196 (1995).
[31] B. H. Bransden and M. R. C. McDowell, *Charge Exchange and the Theory of Ion-Atom Collisions* (Clarendon Press, Oxford, 1992), p. 63-64.
[32] P. C. Stancil, B. Zygelman, and K. Kirby, in *Photonic, Electronic, and Atomic Collisions*, edited by F. Aumayr and H. P. Winter (World Scientific, Singapore, 1998), p. 537.
[33] G. D. Billing and M. Baer, Chem. Phys. Lett. 48, 372 (1977).
[34] H. O. Folkerts, T. Schlathölter, R Hoekstra, and R. Morgenstern, J. Phys. B: At. Mol. Opt. Phys. 30, 5849 (1997).
[35] L. F. Errea, L. Méndez, and A. Riera, J. Phys. B: At. Mol. Phys. 15, 101 (1982).
[36] K. P. Huber and G. Herzberg, *Molecular Spectra and MolecularStructure*, Constants of Diatomic Molecules Vol. 4 (Van Nostrand Reinhold, New York, 1979).
[37] M. B. Shah and H. B. Gilbody, J. Phys. B: At. Mol. Opt. Phys. 23, 1491 (1990).
[38] H. O. Folkerts, F. W. Bliek, M. C. de Jong, R. Hoekstra, and R. Morgenstern, J. Phys. B: At. Mol. Opt. Phys. 30, 5833 (1997).

